Hindawi
Shock and Vibration
Volume 2022, Article ID 3873935, 15 pages
https://doi.org/10.1155/2022/3873935

Research Article

Analysis of Seismic Response of the Arch Bridge across Reservoir considering Fluid-Solid Coupling Effect

Yuhang Chu, Rui Li, and Xiaozhang Li

Faculty of Civil Engineering and Mechanics, Kunming University of Science and Technology, Kunming, Yunnan 650500, China

Correspondence should be addressed to Rui Li; liruiking@kust.edu.cn

Received 29 October 2022; Revised 15 December 2022; Accepted 16 December 2022; Published 26 December 2022

Academic Editor: Letícia Fleck Fadel Miguel

Most of the deep-water bridges in Chinese reservoirs are concentrated on rivers in the southwest region. The unique structural characteristics of arch bridges are more in line with the geological topography requirements of deep reservoir areas, making them the bridge type of choice for bridges in deep reservoir areas. While the southwest region is an earthquake-prone area, in order to study the safety of arch bridges across deep water in the reservoir area, it is necessary to analyze the effect of water under seismic behavior on the box section arch ring and explore the effect of arch inundation depth on the dynamic response of arch bridges in the reservoir area. In this study, the effect of fluid-solid coupling is considered, the modified Morison equation is used to calculate the hydrodynamic pressure, and the effect of arch bridge inundation depth on the dynamic response is analyzed based on the Midas/civil finite element model of the arch bridge in the Yunnan reservoir area. The results show that the seismic response of the arch bridge across the reservoir is greatly influenced by the submergence depth of the arch bridge due to the fluid-solid coupling effect, and the influence of the hydrodynamic pressure on the longitudinal moment (My) and transverse moment (Mz) of the arch bridge increases with the increase of the submergence depth. There is a threshold value of the submergence depth. When the submergence depth is less than the threshold, the effect of fluid-solid coupling is negligible, and when the submergence depth is greater than the threshold, the fluid-solid coupling effect is significant. The thresholds for different parts of the main arch ring are different. The most unfavorable water depth in different parts of the main arch ring is not necessarily the water depth when the arch ring is completely submerged. Based on this result, for reservoir arch bridges in high intensity areas, it is recommended that the inundation depth of arch bridges crossing deep water reservoirs should be h/f less than or equal to 5/8 f.

1. Introduction

To utilize the rich water energy resources in southwest China, a large number of deep reservoir hydropower stations were built. For the purpose of regional economic cooperation and communication, many bridges were built to cross above the reservoir. However, bridges with high pier and deep-water foundation should better be avoided in deep reservoir area, for construction convenience. In all bridge types, the deck arch bridge is mostly preferred, which is in line with the requirements of geological topography and bridge aesthetics. On the other hand, southwest China is an earthquake-prone area. Sevim et al. [1] selected the Osmanli Arch Bridge, also known as the Timisoara Historic Masonry Arch Bridge, to investigate the effects of near- and far-fault ground shaking on the seismic behavior of the historic arch bridge through a combination of numerical and experimental evaluations. The results show that for the stone arch bridge, the effect of near-fault ground shaking on the dynamic behavior is slightly greater than that of far-fault ground shaking, but far-fault ground shaking exhibits a larger peak acceleration. The stress maximum at the bottom of the stone arch bridge is also higher than that at the upper side. The seismic response of the arch bridge in reservoir area would be influenced by the hydrodynamic pressure, and the coupling effects of water and structure should be taken into account in the seismic design [2–4]. The size of the hydrodynamic pressure is closely related to the submerged

depth of the arch [5, 6]. The pier-water coupling analysis methods are divided into three main categories, which are the analytical method, numerical analysis method, and semianalytical seminumerical value method. There are two types of analytical methods: the eigenfunction expansion method [7] and the weighted residual method. In 1933, based on the assumption of the rigid body motion of a structure in an incompressible fluid, Westergaard [8] gave an analytical solution for the dynamic water pressure acting on a rigid vertical dam surface during horizontal seismic vibrations and introduced the concept of "additional mass;" Hogben and Standing [9] solved for the dynamic water pressure on a cylinder immersed in water at the bottom solidified tip under the condition of free surface gravity waves and obtained the analytical solution for the dynamic water pressure. The numerical analysis methods mainly include the finite element method and the boundary element method. The key of the finite element method to solve the coupled problem is the selection of the finite element format and numerical solution scheme for the coupled system. Zeinkiewicz and Newton [10] and his collaborators have carried out incipient work on the finite element format problem for coupled systems. According to the different ways of describing the fluid domain, it can be divided into displacement-displacement format in which the fluid domain is described by a displacement field (Lagrangian method) [11–13] and displacement-pressure format in which the fluid domain is described by a potential function (Eulerian method). In the process of using the Lagrangian method, the problem of "zero-energy mode" often arises, so researchers use methods such as the introduction of the spinless condition of the fluid to eliminate this pathology [14]. There are three main types of semianalytic seminumerical methods: Morison equation method [15], linear radiation wave theory [16], and national norms. Over the past 80 years since 1933, researchers have achieved amazing results. Williams [17] used the Green function to treat the pier-water coupled intersection to investigate the dynamic water pressure on a hollow column in water under high-frequency load excitation. Banerjee and Prasad's [18] study of bridge structures under the combined effects of earthquakes and floods concluded that bridge structures in floods are more susceptible to damage under earthquake action. Yang et al. [19] analyzed the dynamic characteristics of bridge piers in water by means of ANSYS calculations. It was obtained that when the pier was filled with water and under the condition of no water, the 1st order frequency was found to be similar to the 3rd order frequency; the water had a greater influence on the intrinsic vibration frequency of the structure, and the intrinsic vibration frequency decreased gradually with the increase of the water level. Jin et al. [20] established and calculated three-dimensional water-solid coupled finite element modes based on the theory of fluid-solid interface coupling dynamics. It was concluded that the ratio of water depth to pier height has a great influence on the variation scale of pier frequency. Deng et al. [21] constructed a three-dimensional finite element model for a typical deep-water bridge by simulating the fluid-structure interaction between hollow piers and water and the gap element simulating the impact of the gap position, based on the potential-based fluid element. The effects of shock and fluid-structure interaction on long-span deep water bridges with typical high-hollow piers were studied. Zhang et al. [22] argued that hydrodynamic effects are of interest when performing seismic analysis of bridges with complex hollow piers in submerged reservoirs. A typical reservoir bridge with nonuniform hollow piers is used as an example. Linear and nonlinear dynamic analyses were performed to investigate the seismic response of this example abutment under six near-fault and six teleseismic records. The accuracy of the additional mass model was verified in both linear and nonlinear domains. The effects of dynamic water pressure and ground vibration on structural brittleness were investigated by Cui et al. [23]. The results show that dynamic water pressure plays an important role in affecting the conditional failure probability of bridge piers and bearings. The damage probability increases with increasing water depth. At present, the research on the arch bridge in the reservoir area mainly focuses on the determination of the submerged height of the arch bridge, the effect of the submerged depth of the arch bridge on the internal force of the arch bridge, but the research on the dynamic response of arch bridge considering fluid-solid coupling is rarely seen. In this study, the modified Morison equation is used to calculate the hydrodynamic pressure (additional mass), and a bridge in Diqing, Yunnan Province, is taken as an example to conduct seismic analysis. Under the premise of considering the fluid-structure coupling effect, the effects of water on the arch ring with box-shaped section under the action of earthquake are analyzed, and the influence of arch-submerged depth on the dynamic response of arch bridge is explored. The results of this study can provide a reference for seismic design of arch bridges in the deep reservoir area.

2. Modified Morison Formula to Calculate Hydrodynamic Pressure

The formula to calculate hydrodynamic pressure on columnar structure was first proposed by Morison et al. [15]; however, his method ignored the effect of the structure on the fluid, and the new modified Morison formula was later revised as follows [24, 25]:

$$F_D = \frac{\pi}{4}\rho(C_M - 1)D^2(\ddot{u} - \ddot{x}) + \frac{\pi}{4}\rho D^2\ddot{u} + \frac{1}{2}C_D\rho D\left|\dot{u} - \dot{x}_j\right|\left(\dot{u} - \dot{x}_j\right), \tag{1}$$

where $\dot{x}_j$ and $\ddot{x}_j$ are the absolute velocity and acceleration of the columnar structure, respectively; $\dot{u}$ and $\ddot{u}$ are the velocity and acceleration of the water body, respectively; D is the structure diameter; C_D and C_M are the viscous friction resistance coefficient and inertial force coefficient, respectively. It is assumed that the water body is static before the occurrence of earthquake, then, $\dot{u} = \ddot{u} = 0$. The last term of equation (1) is nonlinear; by linearization, equation (1) turns into

$$F_D = -M_W\left(\ddot{x} + \ddot{x}_g\right) - C_W\left(\dot{x} + \dot{x}_g\right),$$
$$M_W = (C_M - 1)\rho V, \quad (2)$$
$$C_W = 0.5C_D\rho A_p\sigma_{\dot{x}+\dot{x}_g}\sqrt{\frac{8}{\pi}},$$

where M_W and C_W are the additional mass matrix and damping matrix of the moving water, respectively; $\dot{x}_g$ and $\ddot{x}_g$ are the ground velocity and acceleration, respectively; $\dot{x}$ and $\ddot{x}$ are the relative velocity and acceleration of the structure, respectively. The damping effect can be neglected according to Yuan's et al. research [26, 27], thus the motion equation of underwater structure is

$$[M + M_W]\ddot{x} + C\dot{x} + Kx = -[M + M_W]\ddot{x}_g. \quad (3)$$

The key point of using Morison formula is to determine the value of C_M. For cylindrical structure, $C_M = 2$ is recommended [28]. While, for structure with slender rectangular cross-section, additional correction factor K_C is required [16]:

$$K_c = 0.94732 + \frac{2.59648}{1 + ((D/B)/0.09516)^{0.54638}}, 0.1 \le \left(\frac{D}{B}\right) \le 10, \quad (4)$$

where D is the side length of the rectangular cross-section perpendicular to the direction of the relative motion and B is the side length of the rectangle parallel to the relative motion edge.

3. The Seismic Analysis considering Fluid-Solid Coupling Effect

The vibration equation of the bridge structure is constructed according to the finite element model. The displacement, velocity, and acceleration responses of the structure are obtained by using the step-by-step integration method, and then, the internal force response of the structure are obtained, accordingly [29]. A general step-by-step formulation was known as Newmark-β method, which is proposed by Newmark. The basic iterative equation for velocity and displacement are expressed as follows:

$$\dot{x}_{t+\Delta t} = \dot{x}_t + [(1-\gamma)\ddot{x}_t + \gamma\ddot{x}_{t+\Delta t}]\Delta t, \quad (5)$$

$$x_{t+\Delta t} = x_t + \dot{x}_t\Delta t + [(0.5-\beta)\ddot{x}_t + \beta\ddot{x}_{t+\Delta t}]\Delta t^2, \quad (6)$$

where γ and β are the adjustable factors, and they are preferred as $\gamma = 1/2$ and $\beta = 1/4$ to make sure of the accuracy and stability of the method. The acceleration at time $t + \Delta t$ can be derived from equation (6):

$$\ddot{x}_{t+t} = \frac{1}{\beta\Delta t^2}\left(x_{t+\Delta t} - x_t\right) - \frac{1}{\beta\Delta t}\dot{x}_t - \left(\frac{1}{2\beta} - 1\right)\ddot{x}_t. \quad (7)$$

By substituting equation (7) into equation (5), the velocity at time $t + \Delta t$ is as follows:

$$\dot{x}_{t+\Delta t} = \frac{\gamma}{\beta\Delta t}\left(x_{t+\Delta t} - x_t\right) + \left(1 - \frac{\gamma}{\beta}\right)\dot{x}_t + \left(1 - \frac{\gamma}{2\beta}\right)\Delta t\ddot{x}_t. \quad (8)$$

The dynamic equilibrium equation of the underwater structure considering the fluid-solid coupling effect at time $t + \Delta t$ is as follows:

$$[M + M_W]\ddot{x}_{t+t} + C\dot{x}_{t+\Delta t} + Kx_{t+\Delta t} = -[M + M_W]\ddot{x}_{g_{t+\Delta t}}. \quad (9)$$

Substituting equations (7) and (8) into equation (9), it can be simplified as

$$\overline{K}x_{t+\Delta t} = \overline{P}_{t+\Delta t}, \quad (10)$$

where

$$\overline{K} = K + \frac{1}{\beta\Delta t^2}\left(M + M_W\right) + \frac{\gamma}{\beta\Delta T}C, \quad (11)$$

and

$$\overline{P}_{t+\Delta t} = -[M + M_W]\ddot{x}_{g_{t+\Delta t}} + (M + M_W)\left[\frac{1}{\beta\Delta t^2}x_t + \frac{1}{\beta\Delta t}\dot{x}_t + \left(\frac{1}{2\beta} - 1\right)\Delta t\ddot{x}_t\right] + C\left[\frac{\gamma}{\beta\Delta t}x_t + \left(\frac{\gamma}{\beta} - 1\right)\dot{x}_t + \left(\frac{\gamma}{2\beta} - 1\right)\Delta t\ddot{x}_t\right]. \quad (12)$$

With equations (7) and (8) and equation (10), the seismic response of the structure under water can be solved.

4. Case Study

The reinforced concrete catenary arch bridge of 140 m span in a reservoir area in northwest of Yunnan Province in China was adopted for analysis. Nearly 2/3 of the main arch, which is of constant box-shaped cross-section, is submerged when the reservoir is filled with water. The spandrel structure and the approach bridge are simple supported T beam bridges of 10 m span. The elevation of half the arch is shown in Figure 1.

The finite element model of the arch bridge was established by Midas/civil software (Figure 2). The finite element model consists of 949 beam elements and 1089 nodes; the foot of the arch and the bottom of the abutment are treated by solidification, and the master-slave rigid connection is established between the column on the arch and the arch ring; the building on the arch is a simply supported beam, and the end restraint is released at the end of each span of the beam to simulate the actual simply supported system. The additional mass of moving water was calculated by the modified Morison equation. The seismic response analysis for the bridge was carried out. According to article 5.3.2 of the Code for Seismic Design of Highway Bridges (JTG/T 2231-01-2020)

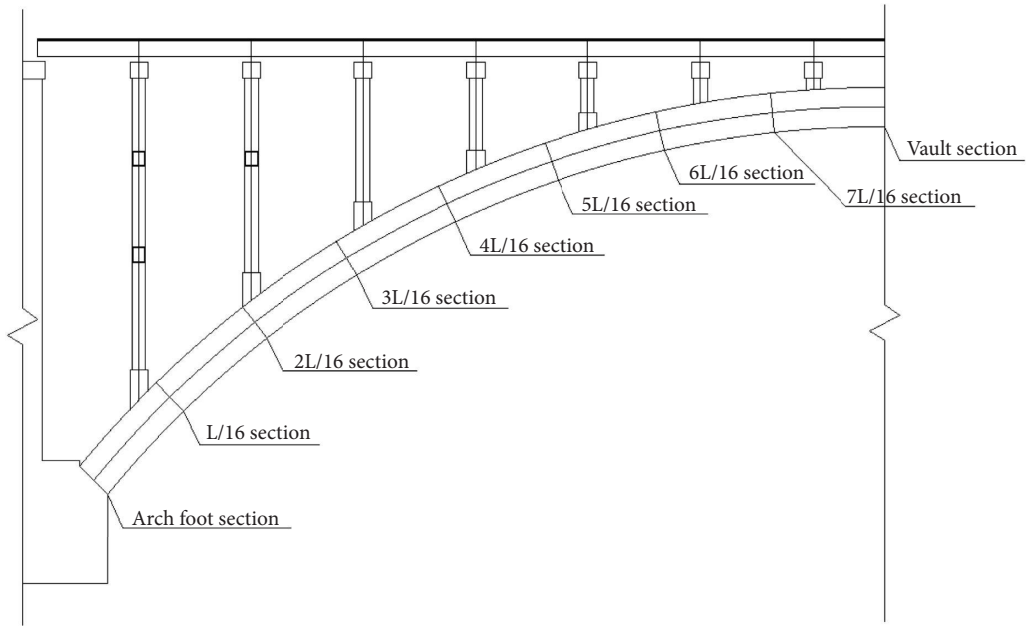

Figure 1: 1/2 arch bridge elevation.

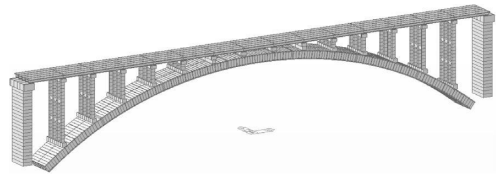

Figure 2: The finite element model of the arch bridge.

[30], bridge project sites that have not been evaluated for seismic safety may be designed with acceleration response spectra according to this code and synthesized with their matching design acceleration time intervals. The actual ground motion acceleration record with the set earthquake magnitude and the distance is generally similar, and the response spectrum is adjusted to match the acceleration response spectrum designed in this specification, and the relative error of the amplitude of the response spectrum corresponding to each cycle value should be less than 5% or the absolute error should be less than 0.01 g.

The design acceleration time range should not be less than three groups and should ensure that the absolute value of the correlation coefficient ρ defined by the equation between any two groups in the same direction time range is less than 0.1.

$$|\rho| = \left| \frac{\sum_j a_{1j} \bullet a_{2j}}{\sqrt{\sum_j a_{1j}^2} \bullet \sqrt{\sum_j a_{2j}^2}} \right|, \tag{13}$$

where a_{1j} and a_{2j} are the values of the jth point of time intervals a_1 and a_2, respectively.

According to the actual engineering of this arch bridge, the maximum value of horizontal design acceleration response spectrum $S_{\max}$ can be obtained as follows:

$$S_{\max} = 2.25 C_i C_s C_d A = 0.2925 g, \tag{14}$$

where C_i is the seismic importance factor, the arch bridge belongs to class B bridge, take $C_i = 1.3$; C_s is the site factor. The arch bridge belongs to class II site, the seismic intensity is 7 degrees, the peak seismic acceleration is 0.1 g, so take $C_s = 1.0$; C_d is the damping adjustment factor, the structural damping ratio is taken as 0.05, and $C_d = 1.0$ is calculated; A is the peak horizontal design fundamental ground acceleration, take $A = 0.1$ g.

According to article 5.1.2 of the Code for Seismic Design of Highway Bridges (JTG/T 2231-01-2020), in general, highway bridges can consider only the horizontal seismic action, and straight-line bridges can consider the seismic action in the direction of X and Y of the horizontal bridge, respectively. The arch bridge belongs to class B bridge, and the seismic intensity in the area is VII degree, so only the horizontal seismic action is considered in the seismic response analysis of the arch bridge. According to the above wave selection principles and then combined with the actual situation in the southwest, two natural real waves and one artificial wave were selected for the peak adjustment, and the selected seismic waves are shown in Figures 3–5. The adjustment of seismic wave parameters is shown in Table 1.

The dynamic analysis of the arch bridge with different inundation depths was carried out under different seismic waves. Due to the large differences in the seismic response at different locations of the arch ring, the arch ring needs to be divided in order to comprehensively analyze the seismic response of the arch ring. The section division is shown in Figure 1 above, and the time courses of the longitudinal moment (My) and transverse moment (Mz) at different locations of the main arch are finally obtained. Figure 6 gives the time history of the longitudinal bending moment (My) at arch foot under the action of seismic wave sfs-48-w in the

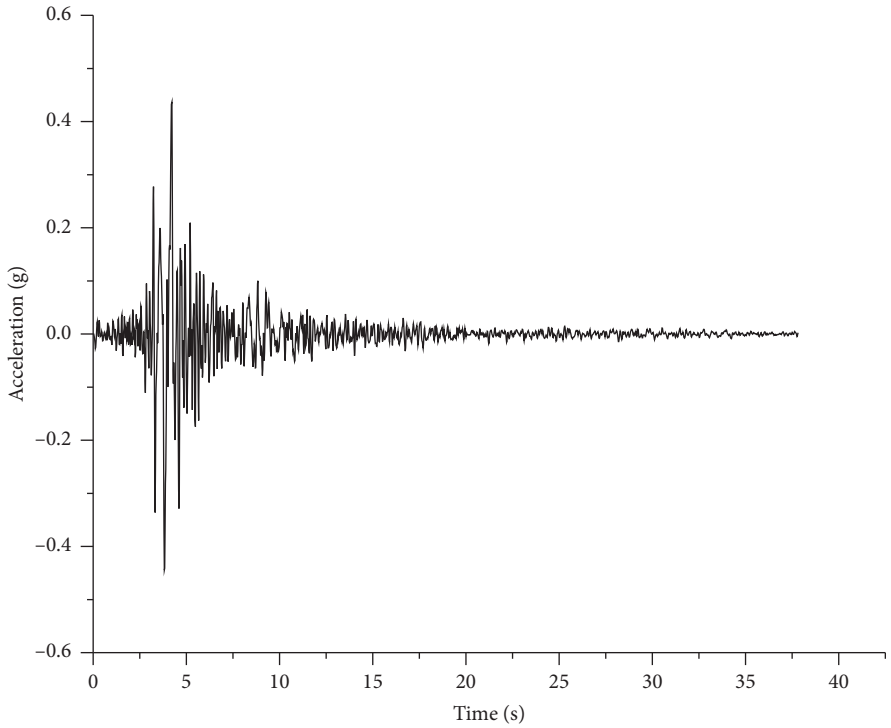

Figure 3: Seismic wave one: sfs-48-w (1987).

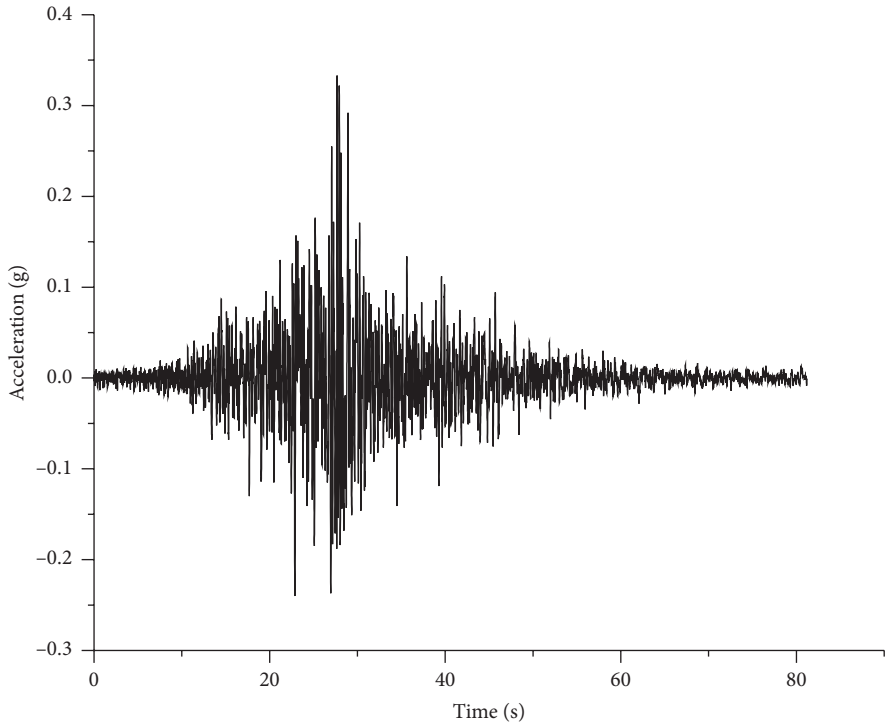

Figure 4: Seismic wave two: san-ew (1985).

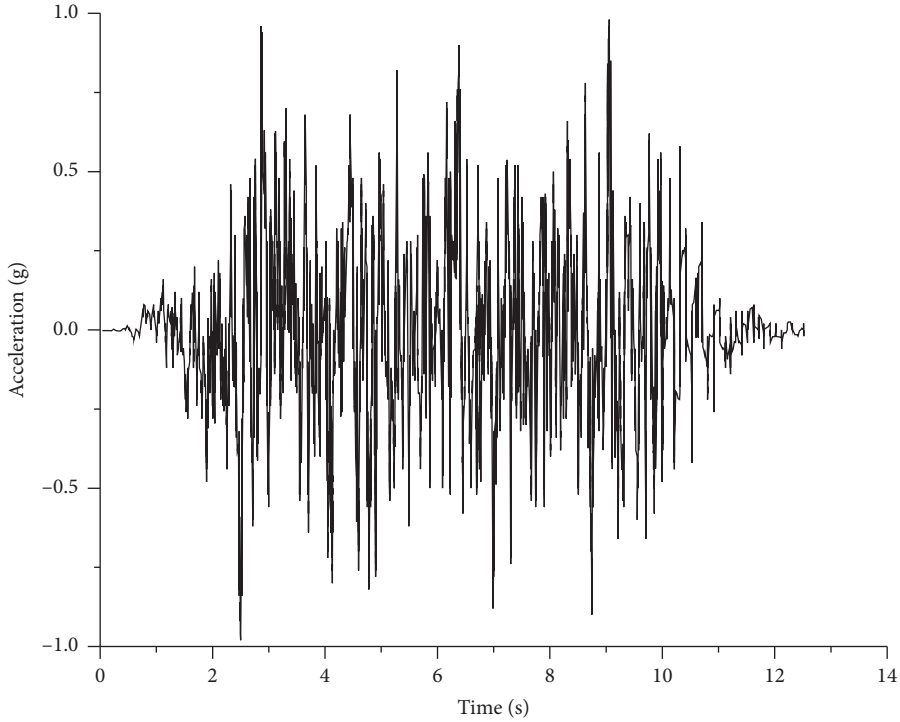

Figure 5: Seismic wave three: artificial seismic wave.

Table 1: Seismic wave parameters adjustment table.

Seismic waves	Basic cycle 10 times	Site characterization cycle	Seismic wave characteristic period (s)	Duration	EPA for waves	Reaction spectrum S_{max} (g)	Reaction spectrum $S_{max}/2.25$ (g)	Peak adjustment factor
TH3TG035sfs-48-w (1987)	8.16	0.40	0.39	9.36	0.38	0.29	0.13	0.35
TH15TG035san-ew (1985)	8.16	0.40	0.42	41.20	0.32	0.29	0.13	0.41
Artificial wave	8.16	0.40	0.44	9.95	0.68	0.29	0.13	0.19

absence of water. In order to explore the effect of the submerged depth of arch on the seismic response of bridge, the peak values of these time histories are processed by

$$R\% = \frac{R_h - R_z}{R_z} \times 100, \tag{15}$$

where R is the influence ratio; R_h is the peak value of bending moments considering fluid-solid coupling effect; and R_z is the peak value of bending moments not considering fluid-solid coupling effect. The influence ratios R at different positions of the main arch with different submerged depth of arch are obtained through equation (14).

After calculation, the relationship between R and submergence depth at different locations of the main arch is shown in Tables 2–10. Figure 7 shows the data plotted in each table.

Figure 7 gives the relation of R and the submerged depth at different positions of the main arch. For illustrative convenience, the horizontal axis represents the ratio of the submergence depth h to the height of arch bridge f. From Figure 7, it can be seen that, for most of the cases, the influence ratio of the fluid-solid coupling effect on My and Mz increases with the submerged depth of arch, and the influence ratio reaches the maximum value when the arch is completely submerged, except for a few cases, the maximum value of influence ratio on My occurs when h = 7/8 f. This is caused by the different seismic response of the main arch to different seismic waves. There seems to be a submerged depth threshold. When the submergence depth is less than the threshold, the influence ratio is small enough to be ignored; but when the submergence depth is greater than the threshold, the influence ratio is significantly increased. The

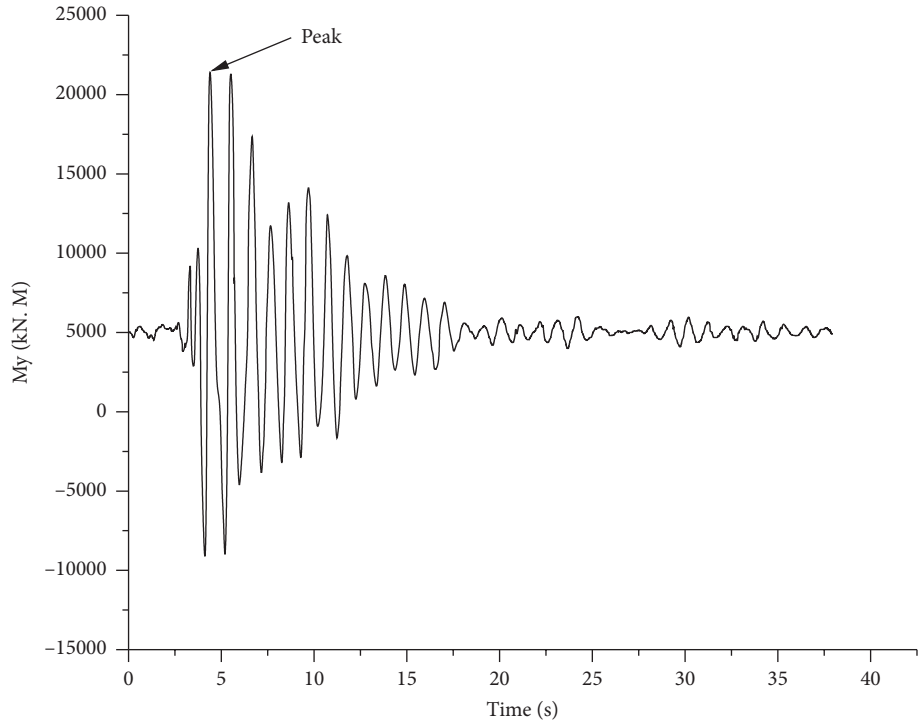

Figure 6: The time history of My at arch foot under the action of seismic wave sfs-48-w in the absence of water.

Table 2: The relation of R and submerged depth at arch foot.

Submerged depth (h/f)	Influence ratio (R%)					
	sfs-48-w (My)	sfs-48-w (Mz)	san-ew (My)	san-ew (Mz)	Artificial wave (My)	Artificial wave (Mz)
1/8	0	0	0	0	0	0
2/8	0.375	0.375	0.375	0.187	1.124	0.562
3/8	1.685	1.498	2.996	0	3.184	1.685
4/8	8.240	3.371	10.112	0.187	−0.375	3.371
5/8	26.217	5.805	22.472	0.187	6.929	5.618
6/8	35.955	8.052	29.026	9.363	28.839	8.802
7/8	88.389	4.119	24.345	10.487	46.629	21.161
8/8	49.438	10.487	43.633	32.209	38.015	35.393

Table 3: The relation of R and submerged depth at L/16 of the arch.

Submerged depth (h/f)	Influence ratio (R%)					
	sfs-48-w (My)	sfs-48-w (Mz)	san-ew (My)	san-ew (Mz)	Artificial wave (My)	Artificial wave (Mz)
1/8	0	0	0	0.081	0.081	0.081
2/8	0.487	0.378	0.270	0.378	1.352	0.487
3/8	1.541	1.432	−0.081	0.892	0.676	1.865
4/8	0.541	2.594	0.000	1.189	2.270	2.811
5/8	4.946	4.405	3.432	1.054	4.189	4.514
6/8	16.054	6.216	15.729	6.216	13.027	6.432
7/8	40.026	5.756	20.135	14.405	51.378	17.000
8/8	55.243	7.351	7.892	31.027	50.810	27.676

Table 4: The relation of R and submerged depth at 2L/16 of the arch.

Submerged depth (h/f)	Influence ratio (R%)					
	sfs-48-w (My)	sfs-48-w (Mz)	san-ew (My)	san-ew (Mz)	Artificial wave (My)	Artificial wave (Mz)
1/8	0.000	0.000	0.000	0.000	0.000	0.000
2/8	2.867	0.000	0.000	0.000	0.000	0.000
3/8	11.470	1.434	1.792	1.434	2.509	1.434
4/8	12.186	3.584	6.093	2.509	5.376	2.867
5/8	11.111	5.735	17.921	2.151	5.376	4.301
6/8	31.541	6.093	22.939	4.660	25.090	1.075
7/8	108.961	7.168	49.104	18.280	103.584	22.939
8/8	139.785	202.151	62.724	31.541	77.778	17.921

Table 5: The relation of R and submerged depth at 3L/16 of the arch.

Submerged depth (h/f)	Influence ratio (R%)					
	sfs-48-w (My)	sfs-48-w (Mz)	san-ew (My)	san-ew (Mz)	Artificial wave (My)	Artificial wave (Mz)
1/8	−0.391	−0.391	−0.391	−0.391	−0.391	−0.782
2/8	0.391	0.000	0.391	0.000	0.000	0.391
3/8	5.869	1.174	1.956	1.174	0.782	1.956
4/8	8.998	3.912	6.651	1.956	4.304	2.739
5/8	10.955	6.651	19.953	1.956	3.130	206.182
6/8	36.385	212.050	1.956	4.304	36.776	200.313
7/8	56.729	222.222	8.216	24.648	40.297	221.831
8/8	3.521	222.613	24.648	32.864	19.171	226.526

Table 6: The relation of R and submerged depth at 4L/16 of the arch.

Submerged depth (h/f)	Influence ratio (R%)					
	sfs-48-w (My)	sfs-48-w (Mz)	san-ew (My)	san-ew (Mz)	Artificial wave (My)	Artificial wave (Mz)
1/8	0.000	0.000	0.064	0.063	−0.438	0.063
2/8	0.627	1.128	0.126	1.128	−0.375	2.130
3/8	−0.312	4.196	0.190	3.195	−0.312	4.697
4/8	−0.250	6.263	5.260	5.261	5.261	5.763
5/8	0.314	9.332	5.323	6.827	3.820	210.234
6/8	7.390	222.320	35.947	0.877	21.919	190.758
7/8	1.441	243.425	23.986	19.977	28.495	224.889
8/8	29.560	240.983	35.571	27.055	64.630	224.952

Table 7: The relation of R and submerged depth at 5L/16 of the arch.

Submerged depth (h/f)	Influence ratio (R%)					
	sfs-48-w (My)	sfs-48-w (Mz)	san-ew (My)	san-ew (Mz)	Artificial wave (My)	Artificial wave (Mz)
1/8	0.000	0.000	0.000	0.000	0.000	0.000
2/8	0.424	0.847	0.424	0.424	1.695	0.847
3/8	2.119	2.542	2.119	2.542	4.237	2.119
4/8	2.966	3.390	4.237	3.390	6.780	3.814
5/8	2.966	5.508	7.203	3.814	6.780	208.051
6/8	5.932	9.746	44.915	8.898	0.847	208.051
7/8	64.831	33.475	40.678	11.864	84.746	239.407
8/8	133.898	34.746	3.814	8.475	106.780	111.017

Table 8: The relation of R and submerged depth at 6L/16 of the arch.

Submerged depth (h/f)	Influence ratio (R%)					
	sfs-48-w (My)	sfs-48-w (Mz)	san-ew (My)	san-ew (Mz)	Artificial wave (My)	Artificial wave (Mz)
1/8	−0.425	−0.425	−0.425	−0.425	−0.425	−0.425
2/8	0.000	0.000	0.000	0.000	0.425	0.425
3/8	2.126	1.276	1.701	1.276	0.850	1.701
4/8	8.929	1.701	0.000	1.701	0.000	2.551
5/8	9.354	3.827	5.527	2.126	5.102	5.527
6/8	2.976	5.102	38.265	3.827	1.276	5.527
7/8	14.881	20.408	39.116	18.708	24.235	24.660
8/8	68.027	25.510	8.503	175.170	50.170	241.922

Table 9: The relation of R and submerged depth at 7L/16 of the arch.

Submerged depth (h/f)	Influence ratio (R%)					
	sfs-48-w (My)	sfs-48-w (Mz)	san-ew (My)	san-ew (Mz)	Artificial wave (My)	Artificial wave (Mz)
1/8	0.029	0.029	0.029	−0.265	0.324	0.324
2/8	1.208	0.619	1.208	0.619	0.913	0.913
3/8	4.742	1.208	1.797	1.797	0.619	1.502
4/8	5.037	2.386	2.680	2.386	3.270	4.742
5/8	2.386	4.153	5.920	1.797	7.099	7.099
6/8	4.153	5.331	25.950	5.037	0.324	6.215
7/8	3.270	18.292	13.873	16.819	5.920	29.779
8/8	8.277	22.710	27.717	169.691	16.819	39.499

Table 10: The relation of R and submerged depth at the vault section.

Submerged depth (h/f)	Influence ratio (R%)					
	sfs-48-w (My)	sfs-48-w (Mz)	san-ew (My)	san-ew (Mz)	Artificial wave (My)	Artificial wave (Mz)
1/8	0.037	0.037	−0.257	0.037	0.037	0.037
2/8	2.720	0.956	0.956	0.368	2.133	0.662
3/8	10.111	1.875	2.463	1.581	2.463	2.169
4/8	20.736	2.500	4.265	1.618	4.853	4.265
5/8	16.067	3.714	6.361	1.654	6.949	6.655
6/8	12.868	4.338	9.926	5.809	5.221	5.809
7/8	24.376	17.905	9.963	30.551	13.198	30.846
8/8	85.294	20.588	49.412	169.411	44.117	38.529

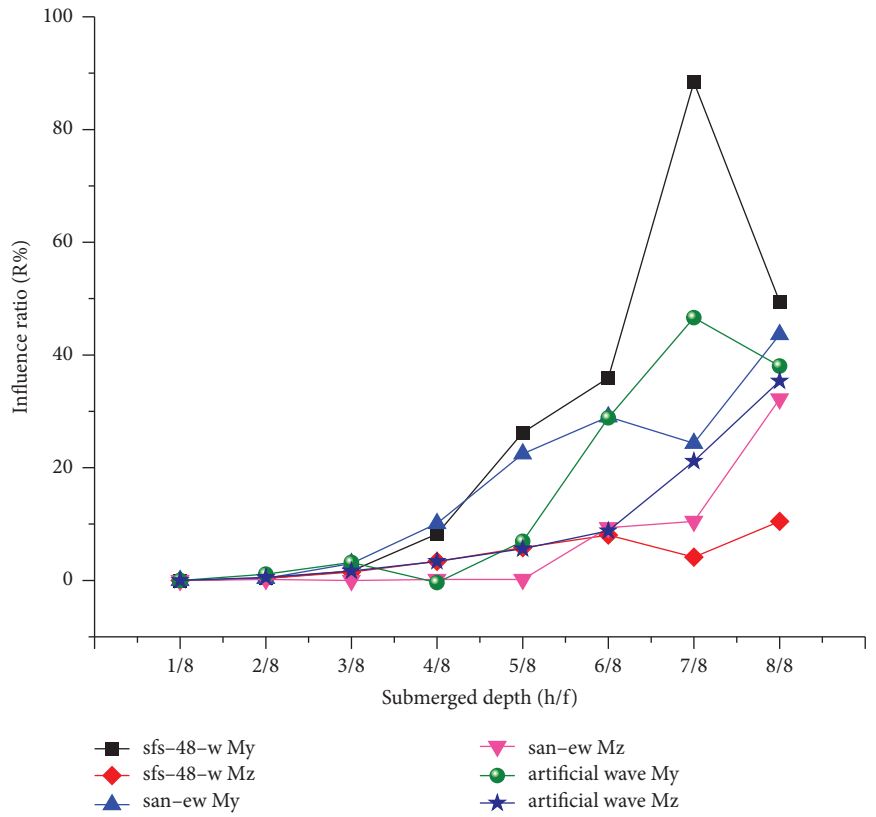

(a)

Figure 7: Continued.

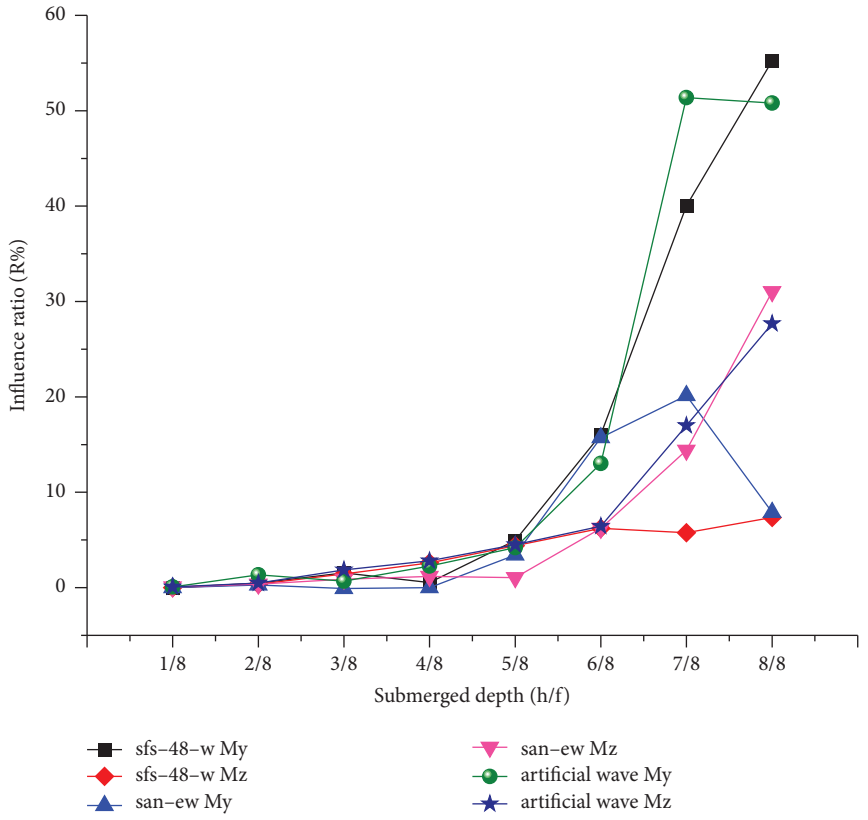

(b)

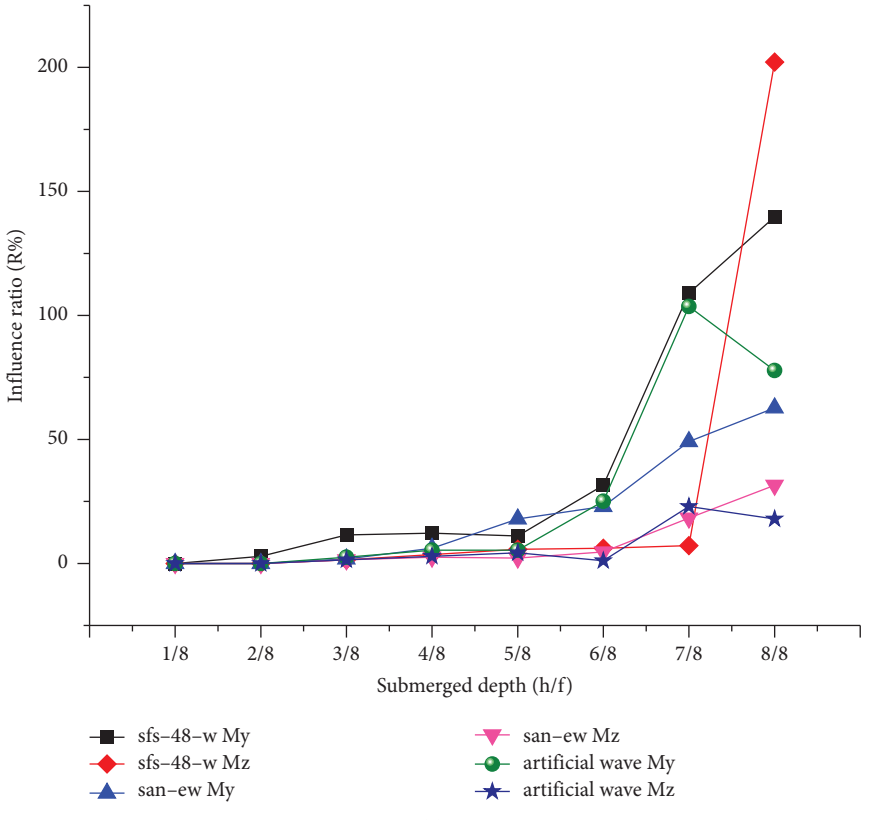

(c)

Figure 7: Continued.

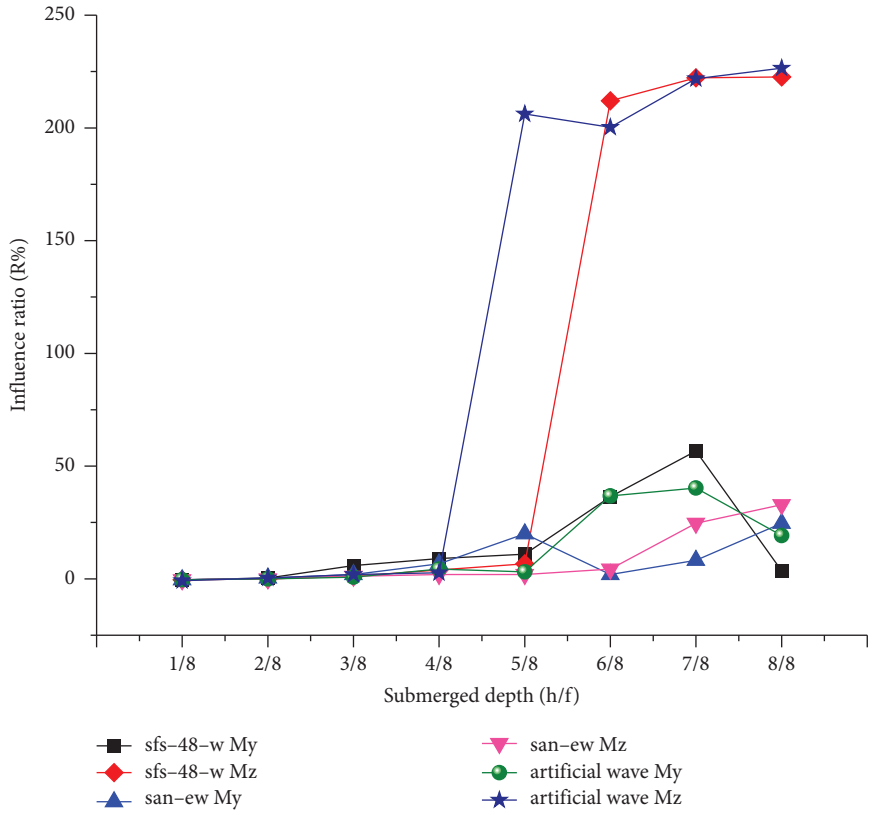

(d)

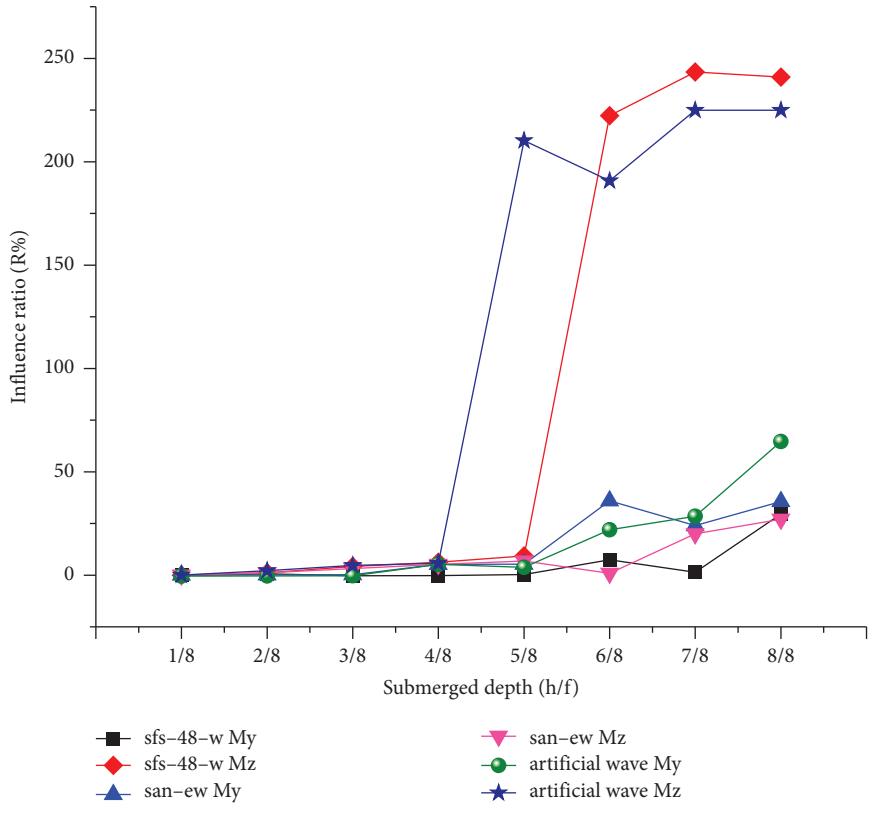

(e)

Figure 7: Continued.

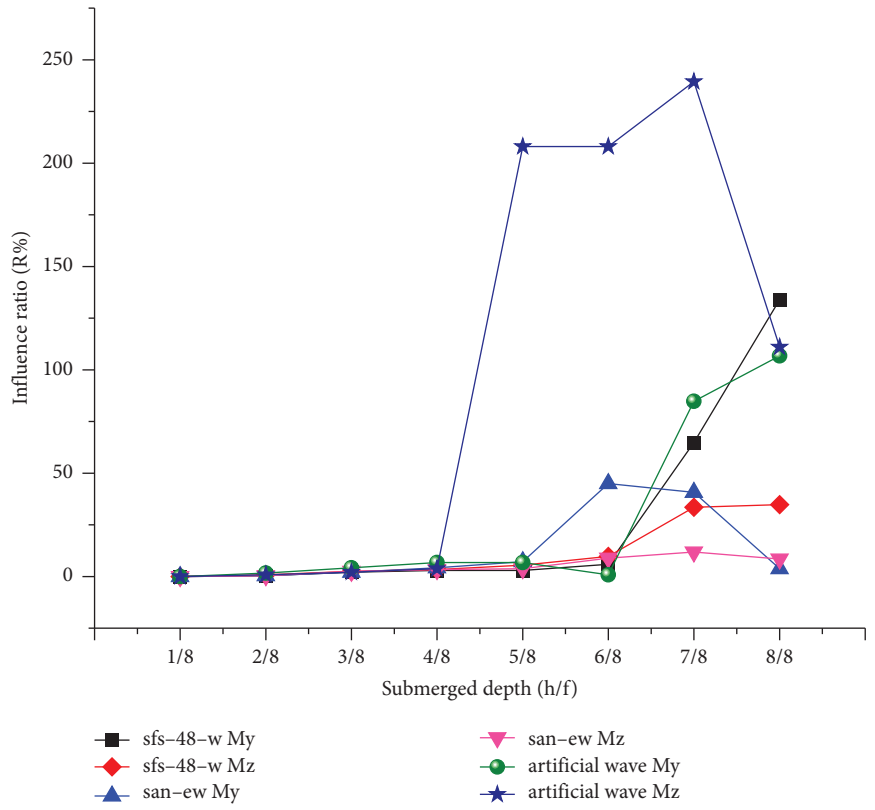

(f)

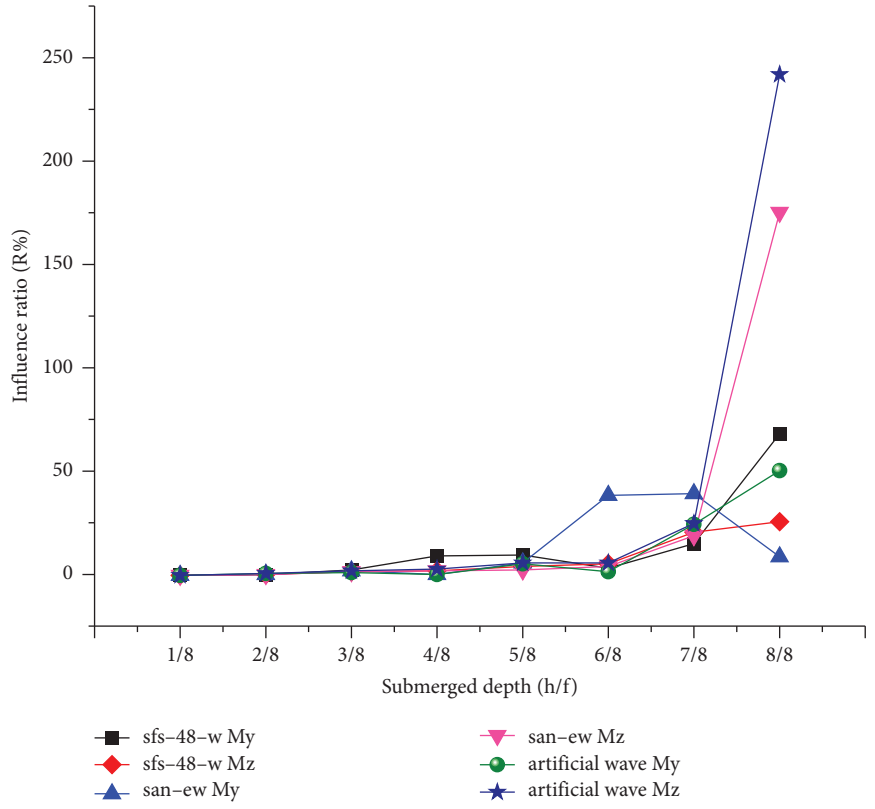

(g)

Figure 7: Continued.

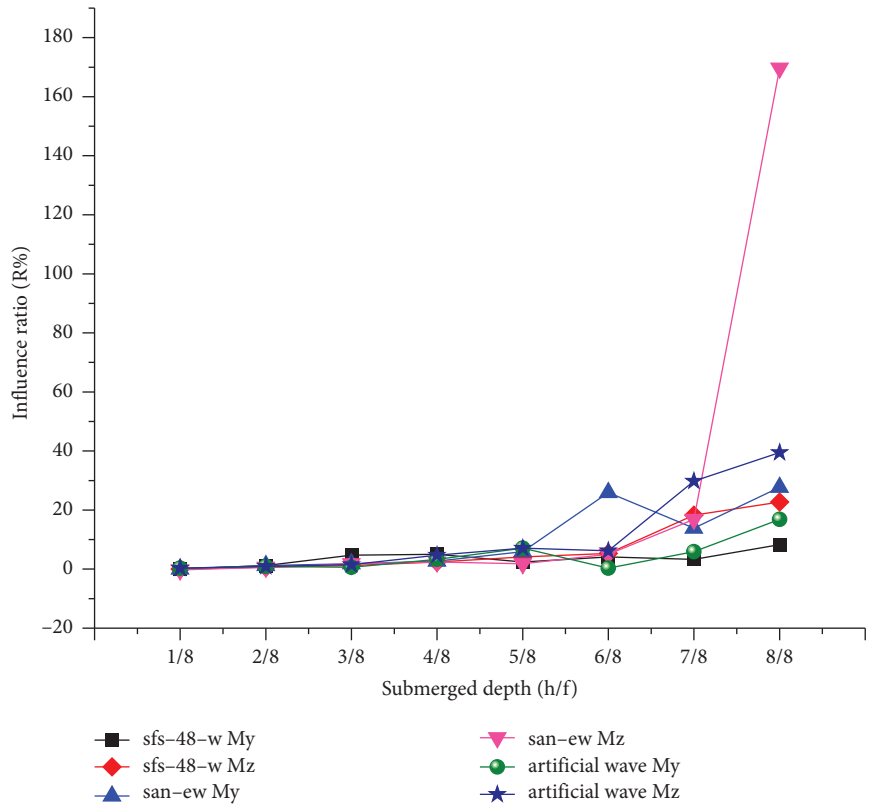

(h)

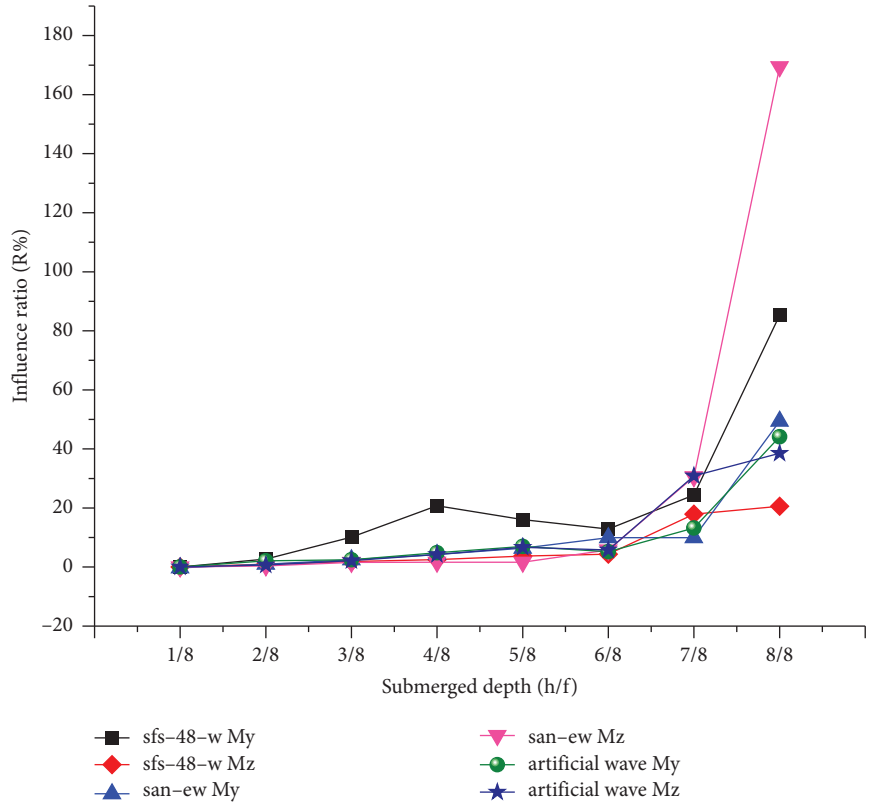

(i)

FIGURE 7: The relation of R and submerged depth at different positions of the main arch. (a) The relation of R and submerged depth at arch foot. (b) The relation of R and submerged depth at L/16 of the arch. (c) The relation of R and submerged depth at 2L/16 of the arch. (d) The relation of R and submerged depth at 3L/16 of the arch. (e) The relation of R and submerged depth at 4L/16 of the arch. (f) The relation of R and submerged depth at 5L/16 of the arch. (g) The relation of R and submerged depth at 6L/16 of the arch. (h) The relation of R and submerged depth at 7L/16 of the arch. (i) The relation of R and submerged depth at the vault section.

Table 11: The threshold and most unfavorable value of the submerged depth.

Internal force	Longitudinal bending moment (My)		Lateral bending moment (Mz)	
Position	Threshold (h/f)	Most unfavorable value (h/f)	Threshold (h/f)	Most unfavorable value (h/f)
Arch foot	4/8	7/8	5/8	Completely submerged
L/16	4/8	7/8	5/8	Completely submerged
2L/16	5/8	7/8	6/8	Completely submerged
3L/16	5/8	7/8	4/8	Completely submerged
4L/16	5/8	Completely submerged	4/8	Completely submerged
5L/16	6/8	Completely submerged	6/8	7/8
6L/16	6/8	Completely submerged	6/8	Completely submerged
7L/16	6/8	Completely submerged	6/8	Completely submerged
Vault section	6/8	Completely submerged	6/8	Completely submerged

L in table is the computed span of arch bridge.

thresholds are not unique for all the circumstances. The submergence depth thresholds and most unfavorable submergence depth for the bending moments at different positions of the arch are given in Table 11.

5. Conclusions

In this paper, by using the modified Morison equation to calculate the hydrodynamic pressure, seismic analysis of an arch bridge in reservoir area considering the fluid-solid coupling effect is conducted. The influence of arch-submerged depth on the dynamic response of arch bridge is explored. The following conclusions are obtained:

(1) The seismic response of arch bridge across reservoir is greatly affected by the submerged depth of arch due to the fluid-solid coupling effect. The influence ratio of fluid-solid coupling effect roughly increases with the submerged depth of arch. The impact ratio reaches a maximum when the arch bridge is completely submerged, except for a few cases, where the impact ratio on My appears as a maximum at $h = 7/8\,f$, which is caused by the different seismic response of the main arch to different seismic waves.

(2) There is a threshold for the submerged depth. When the submerged depth is less than the threshold, the fluid-solid coupling effect is small enough to be ignored. However, when the submerged depth is greater than the threshold, the fluid-solid coupling effect is significant. There are differences in the influence laws of each section of the main arch ring. For reservoir arch bridges in high intensity areas, it is recommended that the submergence depth of arch bridges across reservoirs should be less than $5/8\,f$.

Data Availability

All relevant data used to support the findings of this study are included within the article and are publicly available.

Conflicts of Interest

The authors declare that they have no conflicts of interest.

Acknowledgments

This work was supported by the National Natural Science Foundation of China (Grant No. 51568029) and the Fundamental Research Funds for the Yunnan Communications and Transportation Department (Grant No. 2014(A)5).

References

[1] B. Sevim, S. Atamturktur, A. C. Altunişik, and A. Bayraktar, "Ambient vibration testing and seismic behavior of historical arch bridges under near and far fault ground motions," *Bulletin of Earthquake Engineering*, vol. 14, no. 1, pp. 241–259, 2016.

[2] Y. T. Pang, W. Kai, W. C. Yuan, and G. Shen, "Effects of dynamic fluid-structure interaction on seismic response of multi-span deep water bridges using fragility function method," *Advances in Structural Engineering*, vol. 18, no. 4, pp. 525–541, 2015.

[3] K. Wei, W. C. Yuan, and N. Bouaanani, "Experimental and numerical assessment of the three-dimensional modal dynamic response of bridge pile foundations submerged in water," *Journal of Bridge Engineering*, vol. 18, no. 10, pp. 1032–1041, 2013.

[4] C. G. Liu and G. S. Sun, "Calculation and experiment for dynamic response of bridge in deep water under seismic excitation," *China Ocean Engineering*, vol. 28, no. 4, pp. 445–456, 2014.

[5] C. Y. Liaw and A. K. Chopra, "Dynamics of towers surrounded by water," *Earthquake Engineering & Structural Dynamics*, vol. 3, no. 1, pp. 33–49, 1974.

[6] S. J. Yang, "The seismic behavior of group-pile foundation in deep water," *Electronic Journal of Geotechnical Engineering*, vol. 19, pp. 2679–2690, 2014.

[7] R. P. Han and H. xu, "A simple and accurate added mass model for hydrodynamic fluid-structure interaction analysis," *Journal of the Franklin Institute*, vol. 333, no. 6, pp. 929–945, 1996.

[8] H. M. Westergaard, "Water pressure on dams during earthquakes," *Transactions of the American Society of Civil Engineers*, vol. 98, pp. 929–945, 1933.

[9] N. Hogben and R. G. Standing, "Experience in computing ware loads on large bodies," *Over the Counter*, vol. 2, 1975.

[10] O. C. Zienkiewicz and R. C. Newton, "Coupled vibrations of a structure submerged in a compressible fluid," *Proceedings of the Symposium on Finite Element Techniques*, pp. 98–123, University of Stuttgart, Stuttgart, Germany, 1969.

[11] E. L. Wilson and M. Khalvati, "Finite elements for the dynamic analysis of fluid-solid systems," *International Journal for Numerical Methods in Engineering*, vol. 19, no. 11, pp. 1657–1668, 1983.

[12] W. K. Liu and H. G. Chang, "A method of computation for fluid structure interaction," *Computers & Structures*, vol. 20, no. 1-3, pp. 311–320, 1985.

[13] H. C. Chen and R. L. Taylor, "Vibration analysis of fluid-solid systems using a finite element displacement formulation," *International Journal for Numerical Methods in Engineering*, vol. 29, no. 4, pp. 683–698, 1990.

[14] C. Nitikitpaiboon and K. Bathe, "An arbitrary lagrangian-eulerian velocity potential formulation for fluid-structure interaction," *Computers & Structures*, vol. 47, no. 4-5, pp. 871–891, 1993.

[15] J. R. Morison, J. W. Johnson, and S. A. Schaaf, "The force exerted by surface waves on piles," *Journal of Petroleum Technology*, vol. 2, no. 5, pp. 149–154, 1950.

[16] W. Lai, *Dynamic Response of Deepwater Bridges under Earthquake and Wave*, Tong Ji University, Shanghai, China, 2004.

[17] A. N. Williams, "Analysis of the base-excited response of intake-outlet towers by a green's function approach," *Engineering Structures*, vol. 13, no. 1, pp. 43–53, 1991.

[18] S. Banerjee and G. G. Prasad, "Analysis of bridge performance under the combined effect of earthquake and flood-induced scor," *Vulnerability,Uncertainty,and Risk:Analysis Modeling and Management*, pp. 889–896, 2011.

[19] J. X. Yang, S. R. Zuo, and Y. F. Huang, "Study on fluid-solid coupling analysis method of bridge pier," *Advanced Materials Research*, vol. 594, pp. 1504–1508, 2012.

[20] C. H. Jin, B. M. Zhao, and R. B. Bai, "Analysis of bridge pier's dynamic characteristics considering fluid-solid interface coupling," *Advanced Materials Research*, vol. 1049, pp. 464–468, 2014.

[21] Y. L. Deng, Q. K. Guo, and L. Q. Xu, "Effects of pounding and fluid-structure interaction on seismic response of long-span deep-water bridge with high hollow piers," *Arabian Journal for Science and Engineering*, vol. 44, no. 5, pp. 4453–4465, 2019.

[22] J. R. Zhang, K. Wei, Y. T. Pang, M. Zhang, and S. Qin, "Numerical investigation into hydrodynamic effects on the seismic response of complex hollow bridge pier submerged in reservoir: case study," *Journal of Bridge Engineering*, vol. 24, no. 2, 2019.

[23] S. A. Cui, C. Guo, G. Zeng, L. Xu, J. W. Ju, and H. Jia, "Influence of hydrodynamic pressure on fragility of high-pier continuous rigid frame bridge subjected to ground motion," *Ocean Engineering*, vol. 264, Article ID 112516, 2022.

[24] J. J. Wang, W. Lai, and S. D. Hu, "Hydrodynamic effect on seismic response of bridge. proceedings of the 2nd prc -us workshop on seismic analysis and design of special bridges," Technical Report MCEER-04-0006, pp. 227–244, University at Buffalo, Buffalo, NY, USA, 2004.

[25] W. L. Yang and Q. Li, "The expanded morison equation considering inner and outer water hydrodynamic pressure of hollow piers," *Ocean Engineering*, vol. 69, pp. 79–87, 2013.

[26] Y. C. Yuan, W. Lai, and S. D. Hu, "The effects of hydrodynamic damping on seismic response of bridge piles," *World Earthquake Engineering*, vol. 21, no. 4, pp. 88–94, 2005.

[27] B. F. Chen, "Viscous free surface effect on coastal embankment hydrodynamics," *Ocean Engineering*, vol. 26, no. 1, pp. 47–65, 1998.

[28] China Communications Press, *GB Code of Hydrology for Sea Harbour (JTJ 213-98)*, China Communications Press, Beijing, China, 1998.

[29] R. W. Clough and J. Penzien, *Dynamics of Structures*, Computer & Structures Inc, Berkeley, CA, USA, 2003.

[30] China Communications Press, *Recommended Standards for Industry in the People's Republic of China. Seismic Design Code for Highway Bridges (JTG/T 2231-01-2020)*, China Communications Press, Beijing, China, 2020.